Exp. Theo. NANOTECHNOLOGY 10 (2026) 1237-1253 https://doi.org/10.56053/10.3.1237

Acid-induced corrosion mechanisms of galvanized and non-galvanized steels: Weight loss and EIS analysis with nanotechnology-enhanced surface engineering

Rusul A. Abbas, M. S. Ibrahim[*], *Firas F. Sayyid*

Production Engineering & Metallurgy College, University of Technology- Iraq, Baghdad 10066, Iraq
[*]) Email: rasheed.mohammed40@yahoo.com

Received 21/3/2026, *Received in revised form* 14/5/2026, *Accepted* 24/6/2026, *Published* 15/7/2026

This study systematically evaluated the corrosion behavior and structural evolution of galvanized steel (GS) and low-carbon steel (LCS) in a citric acid medium (pH = 3) using gravimetric, electrochemical, and surface characterization techniques. Weight-loss measurements revealed that GS experienced a marked decrease in corrosion rate with increasing immersion time due to the formation of a protective zinc-based passive layer, whereas LCS showed a gradual increase in corrosion rate, indicating continuous surface degradation. Tafel polarization results confirmed this behavior, with GS exhibiting a more negative corrosion potential and lower effective corrosion activity as a result of enhanced passivation. XRD analysis identified stable $ZnO/Zn(OH)_2$ phases on GS, while LCS primarily formed iron oxide and hydroxide corrosion products. Optical microscopy demonstrated that GS maintained a dense and uniform surface morphology, whereas LCS suffered from pronounced pitting and surface coarsening. FTIR spectra further verified the formation of oxide and hydroxide species on both materials. Overall, galvanized steel showed superior corrosion resistance in acidic environments, highlighting the effectiveness of zinc coatings in protecting low-carbon steel substrates. Additionally, nanotechnology-based approaches such as nanostructured coatings and nanoscale surface modification can further enhance corrosion resistance by improving passive film stability, reducing porosity, and increasing surface uniformity in acidic environments.

Keywords: Tafel; FTIR; Optical; XRD; Nanocoatings.

1. INTRODUCTION

Corrosion of metallic materials is a critical factor affecting the durability, reliability, and economic sustainability of engineering structures [1-5]. Steels operating in acidic environments, including industrial effluents, cleaning agents, and organic acid media, are especially vulnerable to both uniform and localized corrosion [6, 7]. Such degradation leads not only to material loss and reduced mechanical integrity, but also to contamination of surrounding systems and increased maintenance costs [8]. Consequently, the development and evaluation of effective corrosion-resistant materials remain a major focus in materials science and surface engineering [9]. Zinc galvanization is widely recognized as a practical and cost-effective method for improving the corrosion resistance of steel substrates [10]. The zinc coating functions as a sacrificial anode, preferentially dissolving to protect the underlying steel. In corrosive environments, zinc forms adherent and compact layers of zinc oxide (ZnO) and zinc hydroxide ($Zn(OH)_2$), which provide both barrier protection and cathodic shielding [11]. In contrast, low-carbon steel, although inexpensive and widely used, lacks sacrificial protection and is therefore more susceptible to acid-induced corrosion [12,13]. This vulnerability is particularly pronounced in organic acids such as citric acid, which can chelate metal ions and destabilize iron oxide passive films [14]. While numerous studies have examined the corrosion behavior of galvanized steel in strong mineral acids such as HCl and H_2SO_4, significantly fewer investigations have addressed organic acid systems [15,16]. Citric acid represents a chemically complex and environmentally benign medium due to its weak acidity, pH-dependent dissociation, and strong chelating ability, making it especially relevant to food processing, pharmaceutical, and eco-friendly industrial applications [17]. The long-term effectiveness of zinc coatings under such conditions remains insufficiently understood [18]. In this work, the corrosion behavior of galvanized steel and low-carbon steel in citric acid solution (pH = 3) is systematically investigated using gravimetric analysis, Tafel polarization, X-ray diffraction (XRD), Fourier-transform infrared spectroscopy (FTIR), and optical microscopy. Recent advances in nanotechnology have enabled the development of nanostructured coatings and nanoscale surface treatments that significantly improve corrosion resistance. These approaches enhance passive film formation, reduce defect density, and improve adhesion between coating and substrate, offering superior protection compared to conventional galvanization techniques. The study aims to correlate corrosion kinetics, electrochemical parameters, and surface film evolution, thereby providing a scientific basis for material selection and surface protection strategies in mild organic acid environments.

2. MATERIAL AND METHODS

2.1.Materials

Two metallic substrates were used in this investigation: galvanized steel (GS) and low-carbon steel (LCS), both obtained from local industrial suppliers in Iraq and manufactured in China. The GS samples were prepared from hot-dip zinc-coated mild steel sheets (SGCC grade, equivalent to ASTM A653 / EN 10346 DX51D + Z), comprising a low-carbon steel substrate covered with a uniform zinc layer approximately 10–20 μm thick. The base steel contained mainly Fe (≈98–99%), with minor amounts of C (0.05–0.12%), Mn (0.3–0.5%), and trace elements, while the coating consisted of >99% Zn. The LCS substrate (Q195/Q235, equivalent to AISI 1010–1015) was cold-rolled steel with Fe (~99%), C (0.05–0.15%), and Mn (0.25–0.50%). Both materials were machined into 20 × 20 × 1 mm coupons, polished up to 1200-grit SiC paper, cleaned with ethanol, rinsed in deionized water, and air-dried. These substrates were selected to compare sacrificially protected and uncoated steel behavior in citric acid media.

2.2. Solution preparation

The corrosive medium was made using citric acid as the active ingredient. The acidic solution was prepared by dissolving 30 g of citric acid ($C_6H_8O_7$) in 1000 mL of distilled water. The pH of the produced medium was around 3.0, as measured with both a Hach Sension 7 acidity meter and a WTW digital pH meter to guarantee accuracy. During the preparation procedure, a rotating strainer was used to ensure that the acid particles were completely dissolved and distributed evenly throughout the solution. This acidic media was employed in all subsequent corrosion testing under controlled laboratory settings.

2.3. Sample preparation

The raw materials (galvanized and low-carbon steel) were provided in sheet form and machined into tiny specimens ($20 \times 30 \times 1$ mm^3). The sample edges were smoothed using a precision grinding wheel to remove sharp burrs and surface imperfections. Following mechanical preparation, all specimens were carefully washed with distilled water, then cleaned with ethanol to eliminate impurities and oil. The samples were then dried using lint-free tissue and warm air, resulting in a clean and homogeneous surface for corrosion testing. Each specimen was carefully handled to avoid oxidation or contamination before immersion in the citric acid solution.

2.4. Corrosion testing by weight loss method

Prior to immersion, each specimen was carefully weighed using an analytical balance. The materials were then submerged in a citric acid solution containing 30 g/L and a pH of 3.0. Under controlled laboratory circumstances, immersion studies were carried out for exposure durations ranging from 6 to 48 hours. Following each immersion interval, the specimens were carefully removed from the solution, thoroughly rinsed with distilled water to remove any remaining acid, and washed with ethanol to remove any surface contaminants or corrosion products. The cleaned samples were then dried with heated air to ensure that all moisture was completely removed. Finally, each specimen was reweighed using the same analytical balance, and the corrosion rate was estimated using the standard weight loss technique (ASTM G31) by comparing the mass before and after exposure. Figure 1 depicts the practical arrangement of samples during immersion, with labeled specimens (GS and LCS) immersed in an acidic environment created by dissolving 30 g citric acid in 1 L of distilled water. The setup guaranteed constant temperature and aeration conditions throughout the test period (6-48 hours), to correctly measure the weight loss and surface degradation behavior of the materials under same settings [19,20].

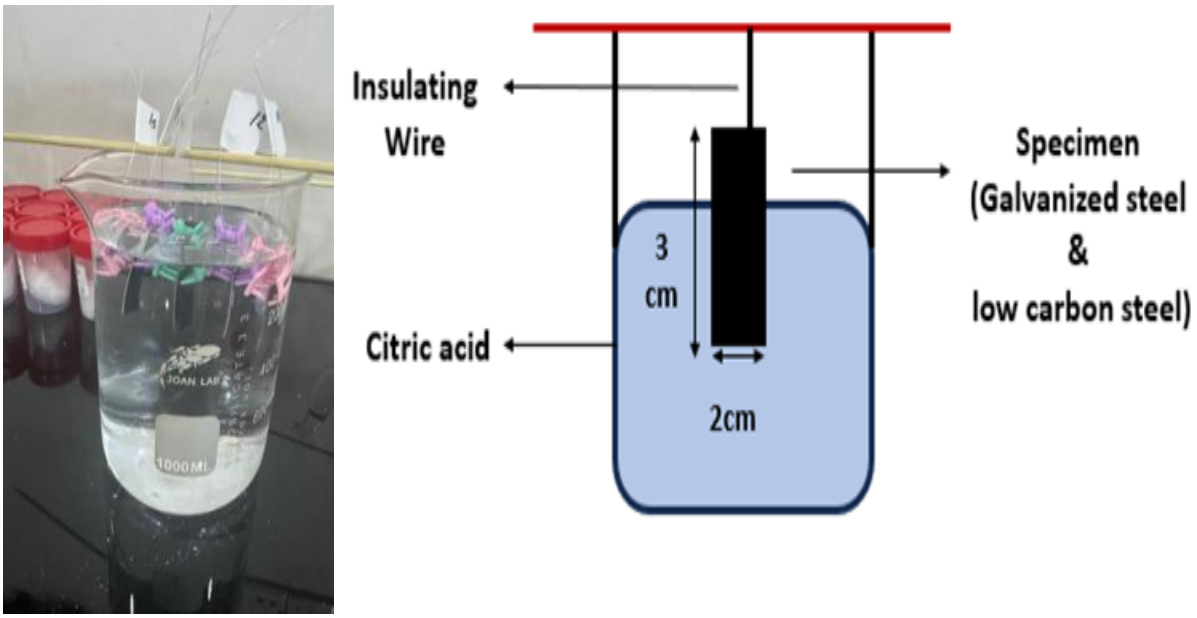

Figure 1 Weight loss experiment setup.

The corrosion rate was calculated using the gravimetric method according to the standard procedures established by the National Association of Corrosion Engineers (NACE). These measurements provided quantitative data on the corrosion performance of galvanized and low-carbon steel in citric acid solution under various exposure times [21-23].

$$C_R = \frac{W}{\alpha t} \quad (1)$$

where: C_R: rate of corrosion, W: weight loss, α: exposed surface area of the sample (cm^2) and t is the period of immersion in hours.

2.5. Electrochemical method

In this work, the electrochemical assessment was undertaken using a Gamry Instrument Potentiostat/Galvanostat/ZRA; having a model of REF 600 instrument, equipped with the DC105 and the EIS300 of Gamry software [19-22]. The working corrosion electrodes were a three-electrode system having a saturated calomel electrode used as the reference electrode, and a freshly cut and cleaned working electrode of metal, having a surface area of 4.5 cm^2 in agreement with the guidelines of ASTM G1-03. The measurements were carried out in citric acid. In terms of importance, the current density when exposure is i when exposure is absence or when is being exposed to the acid. Normally, measurements related to exposure were recorded after the corr(inh) period of time of around 30 min after the electrode is driven across the working electrode dipped within the acidic environment to ensure the ambient reactor is constant at 303 k (Figure 2). The electrochemical measurements comprised of computing the Tafel curves through scanning potential where the spectrum ranges between 0.25 V and +0.25 V SCE and used 0.5 mVs^{-1}. The data acquired from the electrochemical impedance spectroscopy was processed using the appropriate equivalent circuit and the commercially available Gamry Echem Analyst software [23-25].

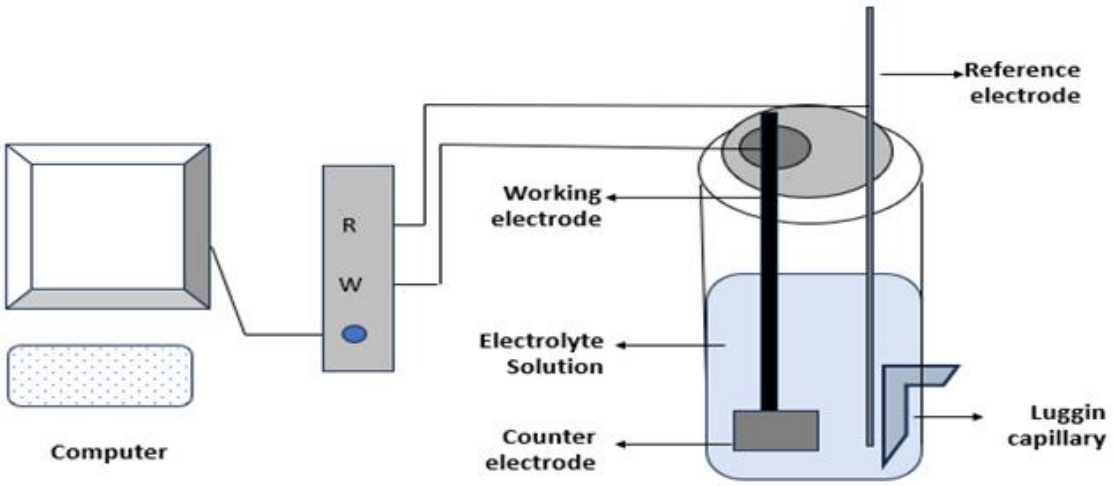

Figure 2 Electrochemical experiment setup.

2.6. Characterization

A comprehensive set of analytical and electrochemical techniques was employed to evaluate the structural, chemical, and corrosion characteristics of galvanized steel (GS) and low-carbon steel (LCS) before and after exposure to citric acid solution. Phase composition and crystallographic changes were analyzed using X-ray diffraction (XRD) with a Bruker D8 Advance diffractometer equipped with Cu Kα radiation (λ = 1.5406 Å), operated at 40 kV and 30 mA. Diffraction patterns were recorded over a 2θ range of 10°–90° with a step size of 0.02°, enabling phase identification and estimation of crystallite size using the Scherrer equation. Fourier-transform infrared spectroscopy (FTIR) was performed using a Shimadzu FTIR-8400S spectrophotometer in the 4000–600 cm^{-1} range with an ATR configuration to identify surface functional groups associated with oxides, hydroxides, and organic residues formed during corrosion. Surface morphology and microstructural evolution were examined using an Olympus BX53M optical microscope at magnifications between 100× and 500× to observe oxide film formation, grain boundary changes, and corrosion pits. Electrochemical behavior was investigated by Tafel polarization using an MLab 200 workstation in a conventional three-electrode cell, employing the steel specimen as the working electrode, a saturated calomel electrode as the reference, and platinum wire as the counter electrode. Corrosion rates were also determined by weight-loss measurements following ASTM G31 procedures.

2.7. Nanotechnology-based surface enhancement

Nanotechnology-based modifications can be introduced through nanoparticle incorporation (e.g., ZnO, TiO_2, Al_2O_3) into coatings or via nanoscale surface treatments. These methods improve coating compactness, enhance electrochemical stability, and reduce corrosion kinetics by limiting ion diffusion pathways in acidic media.

3. RESULTS AND DISCUSSION

3.1. Weight loss method

Table 1 shows the starting and final weights (W_1 and W_2), surface area, immersion duration, and corrosion rates (g/cm^2.h) for galvanized and low-carbon steel samples assessed using the weight loss technique. The corrosion rate was computed based on Eq. 2 [26-29]:

$$Corrosion\ Rate\ (g/cm^2) = \frac{W_1 - W_2}{A \times t} \quad (2)$$

where W_1 and W_2 are the initial and final weights (g), A is the exposed surface area (cm^2), and t is the immersion time (h).

Galvanized steel has increased initial corrosion rates owing to fast oxidation of the zinc coating, followed by a progressive decrease as a compact ZnO/Zn(OH)$_2$ layer develops [30-32]. Low-carbon steel, on the other hand, has a reduced corrosion rate at first but tends to rise significantly with time, indicating the fragility of the thin Fe-oxide layer in the acidic environment. These data confirm the corrosion behavior tendencies seen in Figure 3.

Table 1 Weight loss measurements and computed corrosion rates for galvanized and low-carbon steel specimens in a citric acid media at various immersion periods.

Sample no.	Sample Type	Area (cm^2)	Time (h)	W_1(g)	W_2(g)	Corrosion Rate (g/cm^2·h)
1	Galvanized steel	13	6	4.7725	4.731	5.67×10^{-4}
2	Low carbon steel	13	6	4.5772	4.5728	5.6410×10^{-5}
3	Galvanized steel	13	12	4.3286	4.2851	2.79×10^{-4}
4	Low carbon steel	13	12	4.6715	4.6636	5.0641×10^{-5}
5	Galvanized steel	13	24	4.5965	4.5339	2.01×10^{-4}
6	Low carbon steel	13	24	4.3576	4.3391	5.0641×10^{-5}
7	Galvanized steel	13	48	4.327	4.2468	1.29×10^{-4}
8	Low carbon steel	13	48	4.7515	4.7115	6.41026×10^{-5}

Figure 3 illustrates the variation in corrosion rate (g/cm^2·h × 10^{-4}) of galvanized steel (GS) and low-carbon steel (LCS) as a function of immersion time in citric acid solution. Distinct corrosion behaviors are observed for the two materials, primarily due to the presence of the zinc protective coating on GS. During the initial immersion stage (≤10 h), GS exhibits a relatively high corrosion rate (~5.8 × 10^{-4} g/cm^2·h), attributed to the rapid dissolution of the outer zinc layer and removal of loosely adhered surface films [33-35]. In contrast, LCS shows a lower initial rate (~3.0 × 10^{-4} g/cm^2·h) owing to the temporary formation of a thin native iron oxide layer that delays metal dissolution. Between 10 and 24 h, both materials experience a decrease in corrosion rate [36, 37]. For GS, this reduction results from the formation of a dense and adherent ZnO/Zn(OH)$_2$ layer that enhances surface passivation, while LCS reaches a minimum corrosion rate due to transient iron hydroxide formation [38]. Beyond 24 h, corrosion behavior diverges markedly: LCS exhibits a progressive increase in corrosion rate, reaching ~6.5 × 10^{-4} g/cm^2·h after 50 h, indicating passive film breakdown and localized corrosion. Conversely, GS continues to show a gradual decline, attaining ~1.5 × 10^{-4} g/cm^2.h, confirming sustained zinc-based protection [39-41].

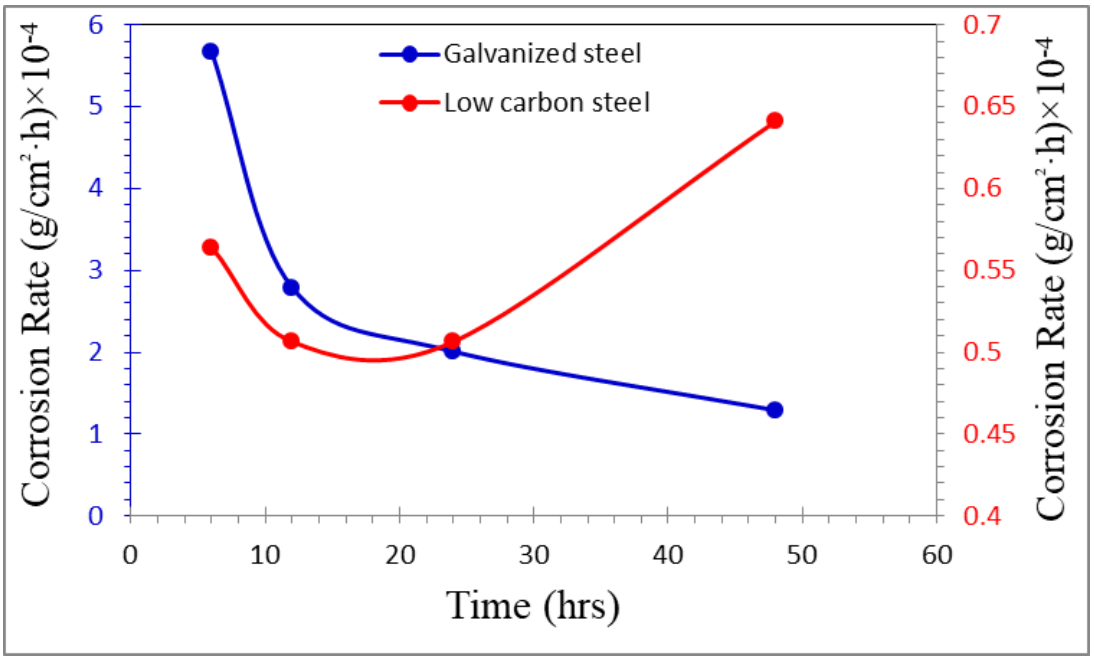

Figure 3 Variation of corrosion rate with immersion time for galvanized and low-carbon steel specimens in citric acid medium, determined by the weight loss method.

3.2. Electrochemical measurements

Figure 4 presents the Tafel polarization behavior of the galvanized steel (GS) specimen immersed in citric acid solution, as obtained from the electrochemical workstation. The polarization curve exhibits well-defined anodic and cathodic branches, whose intersection corresponds to the corrosion potential (E_{corr}) and corrosion current density (I_{corr}), which are fundamental parameters for evaluating corrosion kinetics. From the extrapolated Tafel lines, Ecorr was determined to be approximately −974.3 mV (vs. reference electrode), while I_{corr} was about 42.9 μA/cm^2. The anodic ($\beta_a \approx 82.7$ mV/dec) and cathodic ($\beta_c \approx 83.7$ mV/dec) Tafel slopes are nearly symmetrical, indicating a mixed-type corrosion control in which both anodic zinc dissolution and cathodic hydrogen evolution reactions are simultaneously influenced. The relatively negative E_{corr} value confirms the sacrificial behavior of the zinc coating, which preferentially oxidizes and protects the underlying steel substrate. The anodic branch is associated with zinc oxidation ($Zn \rightarrow Zn^{2+} + 2e^-$), whereas the cathodic branch corresponds to hydrogen ion reduction ($2H^+ + 2e^- \rightarrow H_2$). The moderate Icorr value reflects a controlled corrosion rate, consistent with the formation of protective ZnO and $Zn(OH)_2$ surface films. The linearity of the Tafel regions and the clear intersection point suggest stable electrochemical behavior with minimal disruption of surface passivation. These results are in good agreement with the weight-loss data, further confirming the enhanced corrosion resistance of galvanized steel in acidic media [42-45].

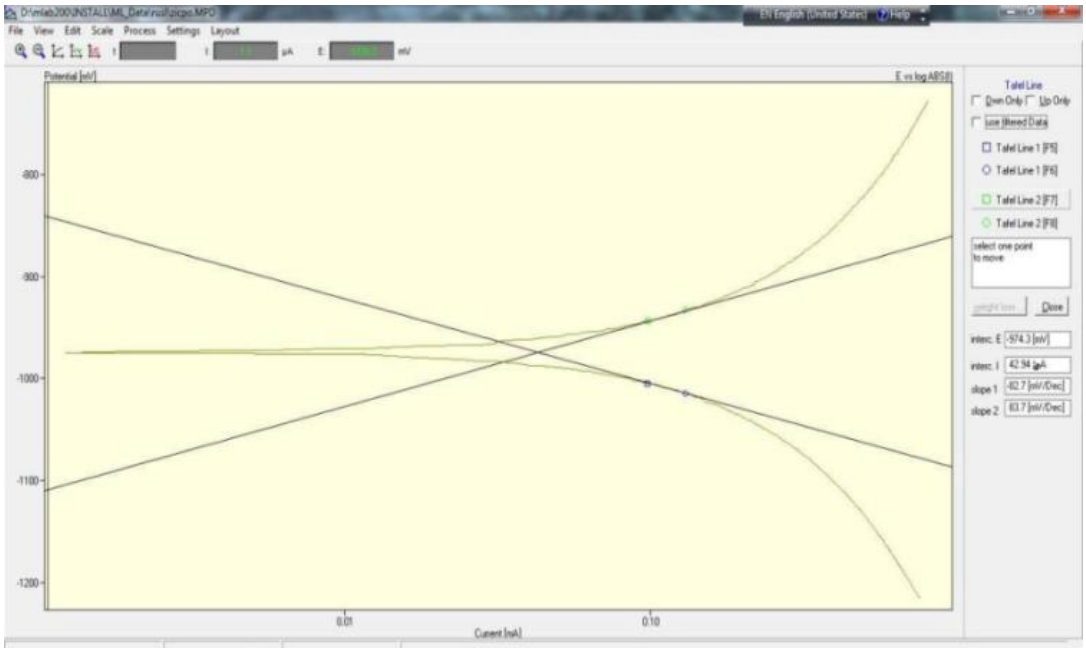

Figure 4 Galvanized steel Tafel.

Figure 5 shows the Tafel polarization curve of low-carbon steel (LCS) immersed in citric acid solution, displaying well-defined anodic and cathodic branches that intersect at the corrosion potential (E_{corr}) and corrosion current density (I_{corr}) [32-35]. From Tafel extrapolation, E_{corr} was determined to be approximately −461.5 mV, while I_{corr} was about 23.28 µA/cm^2. The anodic ($\beta_a \approx 97.2$ mV/dec) and cathodic ($\beta_c \approx 67.1$ mV/dec) Tafel slopes indicate a mixed-control corrosion mechanism with a slightly dominant anodic process. The comparatively less negative E_{corr} value, relative to galvanized steel (−974.3 mV), suggests that LCS is electrochemically more noble but lacks sacrificial protection. The anodic branch corresponds to iron dissolution ($Fe \rightarrow Fe^{2+} + 2e^-$), whereas the cathodic branch represents hydrogen evolution ($2H^+ + 2e^- \rightarrow H_2$). The relatively low initial I_{corr} implies the temporary formation of a thin iron oxide/hydroxide film (Fe_2O_3, Fe_3O_4, $Fe(OH)_2$), which provides short-term passivation [46-50]. However, this layer is porous and unstable in acidic media, leading to progressive breakdown and localized corrosion during prolonged exposure. Compared with galvanized steel, LCS exhibits a higher long-term corrosion tendency due to the absence of a protective zinc layer, consistent with the weight-loss results shown in Figure 3.

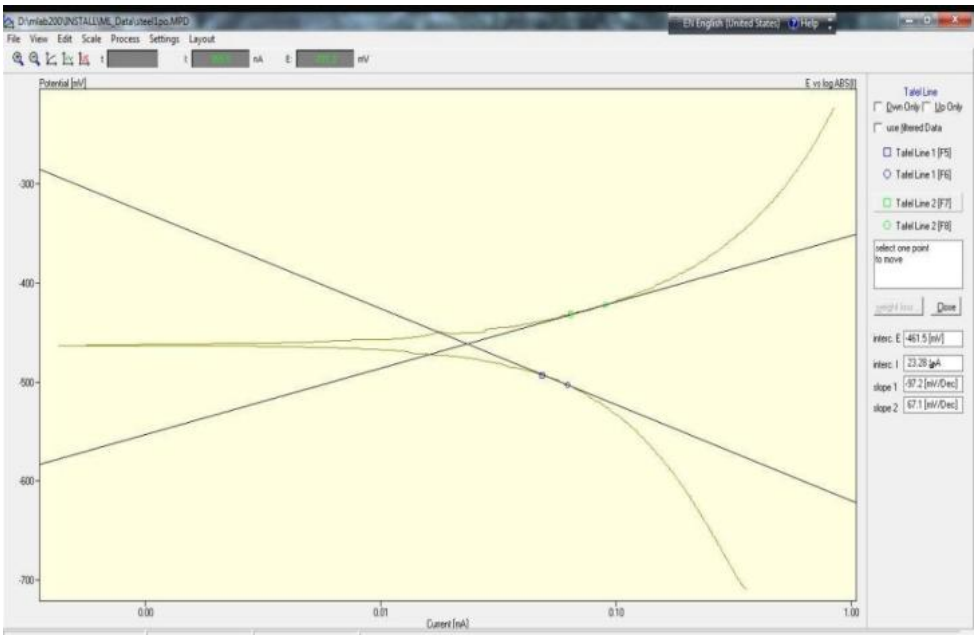

Figure 5 Tafel polarization curve of low-carbon steel in citric acid medium.

3.3. Optical microscope

Figure 6 illustrates the surface morphology evolution of galvanized steel (GS) and low-carbon steel (LCS) before and after immersion in citric acid and subsequent electrochemical polarization [36-40]. As shown in Fig. 6(a), the as-received GS surface is smooth and homogeneous, with well-defined polishing marks and uniformly distributed zinc grains, indicating a dense and adherent Zn coating free of defects. In contrast, Fig. 6(b) shows that LCS exhibits a typical ferritic–pearlitic microstructure without any protective coating, rendering it inherently more susceptible to acidic attack. After 6 h of immersion, Fig. 6(c) reveals the appearance of fine, uniformly distributed dark granules on the GS surface, attributed to the initial formation of zinc hydroxide and zinc–citrate compounds, while the metallic luster is largely preserved. Under the same conditions, Fig. 6€ shows that LCS develops localized dark regions and slight surface roughening due to Fe^{2+} dissolution and the onset of micro-pitting along grain boundaries [51-55]. After 48 h, Fig. 6(d) indicates that GS is fully covered by a compact $ZnO/Zn(OH)_2$ layer, enhancing passivation. Conversely, Fig. 6(f) demonstrates severe degradation of LCS, with porous, flaky corrosion products. Following Tafel polarization, Fig. 6(g) confirms the formation of a refined, adherent ZnO passive film on GS, whereas Fig. 6(h) reveals extensive pitting and poor oxide adherence on LCS, highlighting the superior protective behavior of zinc coatings.

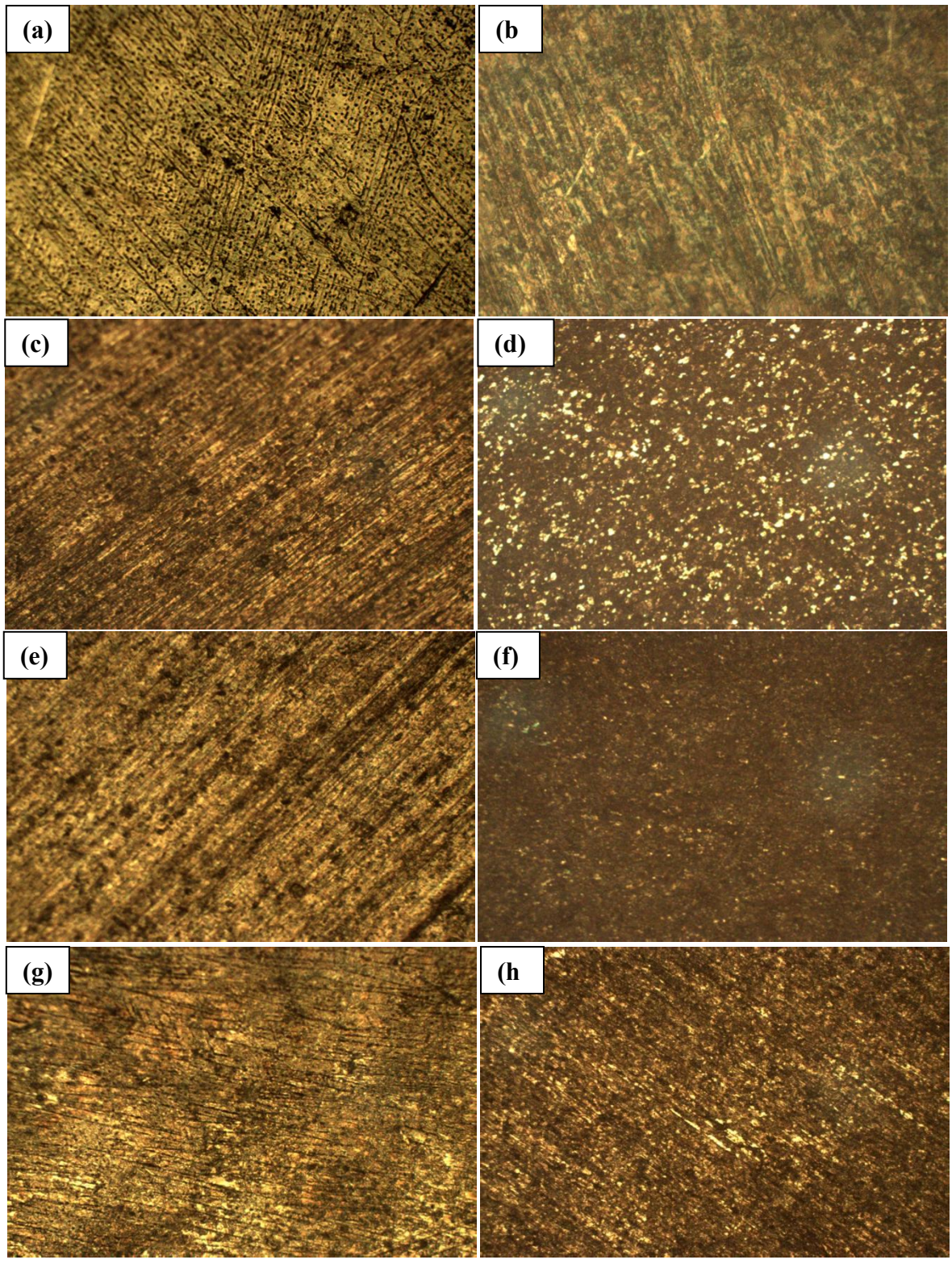

Figure 6 Optical microscope photographs of galvanized steel (GS) and low-carbon steel (LCS) surfaces before and after immersion in citric acid (pH = 3), followed by Tafel polarization (a) As-received GS; (b) As-received LCS; (c) GS after 6 h immersion (GSCa-6 h); (d) GS after 48 h

immersion (GSCa-48 h); (e) LCS after 6 h immersion (LCSCa-6 h); (f) LCS after 48 h immersion (LCSCa-48 h); (g) GS after Tafel polarization (GSCaT); and (h) LCS after Tafel polarization (LCSCaT).

3.4. XRD

Figure 7 presents the X-ray diffraction (XRD) patterns of galvanized steel (GS) and low-carbon steel (LCS) after exposure to citric acid (pH = 3), revealing clear structural differences as a function of immersion time and electrochemical treatment. The as-received GS sample exhibits intense reflections at 2θ ≈ 36.3°, 39.0°, 43.3°, and 54.3°, corresponding to the (002), (100), (101), and (103) planes of hexagonal close-packed Zn (JCPDS 04-0831), confirming the presence of a well-crystallized and continuous zinc coating with negligible contribution from the Fe substrate. After 6 h of immersion, weak additional peaks appear at 2θ ≈ 31.7° and 34.4°, indexed to ZnO (JCPDS 36-1451), indicating initial surface oxidation through controlled Zn dissolution and re-precipitation as $Zn(OH)_2$/ZnO. With prolonged immersion (24–48 h), ZnO reflections become more pronounced while metallic Zn peaks remain detectable, suggesting the development of a stable mixed Zn/ZnO passive layer. Narrower diffraction peaks and increased crystallite size (up to ~25 nm) further indicate improved oxide crystallinity and structural stability. In contrast, LCS displays characteristic α-Fe (bcc) reflections at 2θ ≈ 44.7°, 65°, and 82° (JCPDS 06-0696). Short-term immersion causes slight peak broadening, while longer exposure leads to reduced intensity and faint features near 33–35°, associated with Fe_2O_3 and FeOOH formation. Increased FWHM and reduced crystallite size (~17 to ~13 nm) indicate lattice distortion and microstrain caused by active corrosion. After Tafel polarization, GS shows intensified ZnO peaks, confirming electrochemically driven passivation, whereas LCS mainly exhibits weakened α-Fe reflections, evidencing continued dissolution. These results confirm the superior structural stability and protective nature of zinc coatings in citric acid environments [56-60].

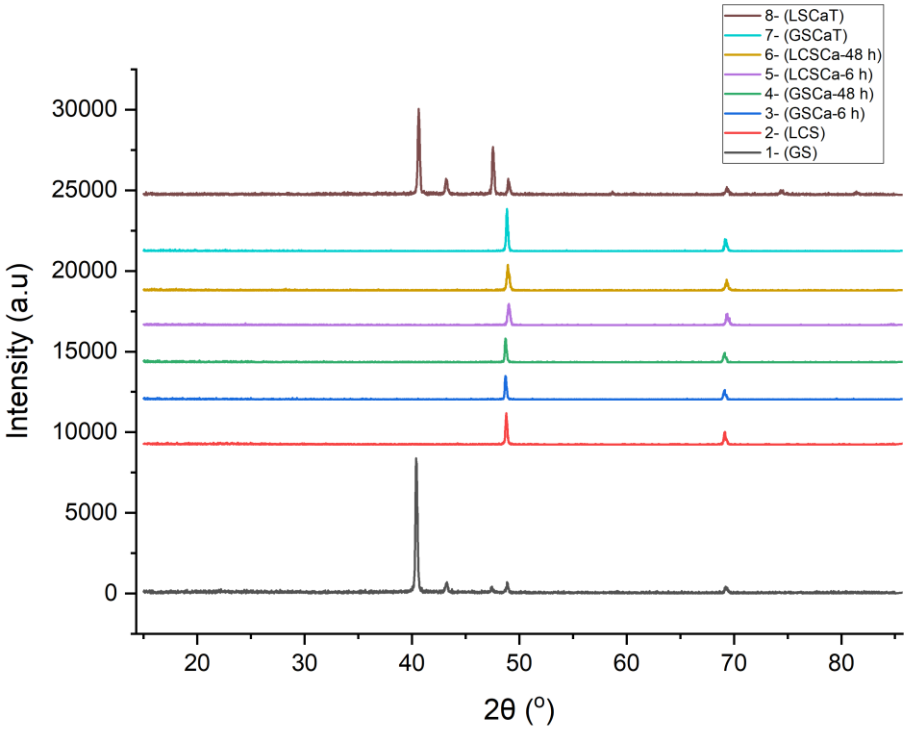

Figure 7 XRD pattern of (GS) and (LCS) surfaces before and after immersion in citric acid (pH ≈ 3) and following Tafel polarization. (a) As-received GS; (b) As-received LCS; (c) GS after 6 h immersion (GSCa-6 h); (d) GS after 48 h immersion (GSCa-48 h); (e) LCS after 6 h immersion (LCSCa-6 h); (f) LCS after 48 h immersion (LCSCa-48 h); (g) GS after Tafel polarization (GSCaT); and (h) LCS after Tafel polarization (LCSCaT).

Table 2 summarizes the X-ray diffraction (XRD) parameters of galvanized steel (GS) and low-carbon steel (LCS) samples before immersion, after exposure to citric acid, and following electrochemical (Tafel) polarization, including diffraction planes (hkl), 2θ positions, interplanar spacing (d_{hkl}), full width at half maximum (FWHM), estimated crystallite size, identified phases, and corresponding JCPDS reference cards. The results indicate that GS exhibits characteristic reflections of metallic Zn (JCPDS 04-0831) and ZnO (JCPDS 36-1451), demonstrating a progressive transformation of the zinc coating into a protective ZnO layer with increasing immersion time. In contrast, LCS predominantly shows α-Fe (BCC) reflections (JCPDS 06-0696), with minor contributions from Fe_2O_3 and FeOOH (JCPDS 39-1346 and 29-0713) appearing after prolonged exposure, indicating limited but unstable oxidation. The gradual increase in FWHM accompanied by a reduction in crystallite size from approximately 45 nm to 28 nm reflects lattice distortion, microstrain development, and the formation of nanocrystalline oxide phases during corrosion. After Tafel polarization, GS retains sharp and well-defined diffraction peaks, confirming the formation of a stable and crystalline ZnO-based passive layer, whereas LCS displays broadened oxide-related peaks with reduced crystallinity, consistent with porous and weakly adherent corrosion products. Overall, the XRD analysis confirms that zinc coatings promote durable passivation and structural stability, while uncoated low-carbon steel undergoes progressive microstructural degradation in citric acid environments [61-63].

Table 2 XRD pattern, phases, and crystallite sizes for galvanized and low-carbon steel samples.

Sample	(hkl)	2θ (°)	d_{hkl} (Å)	FWHM (°)	Crystallite Size (nm)	Phase	JCPDS Card No.
1 – Galvanized Steel (GS)	(002)	36.3	2.47	0.20	45	Zn (metal)	04-0831
	(100)	39.0	2.31	0.22	42	Zn (metal)	04-0831
	(101)	43.4	2.08	0.24	40	Zn (metal)	04-0831
2 – Low Carbon Steel (LCS)	(110)	44.7	2.03	0.18	55	α-Fe (ferrite)	06-0696
	(200)	65.0	1.43	0.20	50	α-Fe (ferrite)	06-0696
	(211)	82.3	1.17	0.22	47	α-Fe (ferrite)	06-0696
3 – GSCa-6 h	(110)	44.7	2.03	0.25	38	α-Fe + FeOOH (trace)	06-0696 / 29-0713
	(200)	65.0	1.43	0.27	36	α-Fe	06-0696
	(211)	82.3	1.17	0.28	35	α-Fe	06-0696
4 – GSCa-48 h	(002)	36.3	2.47	0.28	35	ZnO / $Zn(OH)_2$	36-1451
	(100)	39.0	2.31	0.29	33	Zn (metal)	04-0831
	(101)	43.3	2.09	0.30	32	Zn + Fe (overlap)	04-0831 / 06-0696
	(200)	65.0	1.43	0.30	31	Fe (ferrite)	06-0696
5 – LCSCa-6 h	(110)	44.7	2.03	0.26	38	α-Fe	06-0696
	(200)	65.0	1.43	0.28	36	α-Fe	06-0696
	(211)	82.3	1.17	0.29	33	α-Fe	06-0696
6 – LCSCa-48 h	(002)	36.3	2.47	0.32	32	ZnO / Fe_2O_3 (oxide mixture)	36-1451 / 39-1346
	(100)	39.0	2.31	0.34	30	Zn (metal)	04-0831
	(101)	43.3	2.09	0.35	29	Fe + Zn (overlap)	06-0696 / 04-0831
	(200)	65.0	1.43	0.35	28	Fe (ferrite)	06-0696
7 – GSCaT	(110)	44.7	2.03	0.22	45	α-Fe (ferrite)	06-0696
	(200)	65.0	1.43	0.23	43	α-Fe (ferrite)	06-0696
	(211)	82.3	1.17	0.24	41	α-Fe (ferrite)	06-0696
8 – LCSCaT	(100)	31.7	2.82	0.35	27	ZnO (wurtzite)	36-1451
	(002)	34.4	2.60	0.36	26	ZnO (wurtzite)	36-1451
	(101)	36.3	2.47	0.37	25	ZnO (wurtzite)	36-1451
	(110)	43.2	2.09	0.38	24	Zn + Fe (overlap)	04-0831 / 06-0696
	(103)	54.3	1.69	0.38	24	Zn (metal)	04-0831

3.5. FTIR

Figure 8 presents the FTIR transmittance spectra (4000–400 cm^{-1}), revealing the evolution of surface chemistry and corrosion products on galvanized steel (GS) and low-carbon steel (LCS) during immersion and polarization in citric acid. The as-received GS sample shows an almost featureless baseline, indicating a predominantly metallic zinc surface with only weak O–H (~3400 cm^{-1}) and H–O–H (~1630 cm^{-1}) bands from adsorbed moisture. In contrast, the untreated LCS exhibits Fe–O stretching vibrations at 560–580 cm^{-1}, confirming the presence of a thin native iron oxide layer. After 6 and 48 h of immersion, GS develops new absorptions in the 1100–1000 cm^{-1} region attributed to Zn–O–C/Zn–OH–C bonds, together with intensified Zn–O (430–460 cm^{-1}) and O–H bands, indicating progressive formation of ZnO/$Zn(OH)_2$ and zinc–citrate complexes. LCS, however, shows strong Fe–O and Fe–O–H bands (500–600 cm^{-1}) and carbonate features at 1410–1460 cm^{-1}, associated with

FeOOH and Fe_2O_3 formation. Following Tafel polarization, GS exhibits sharper Zn–O peaks and reduced hydroxyl absorption, signifying a dense, crystalline ZnO passive film, whereas LCS displays broad O–H and Fe–O–H bands characteristic of hydrated, porous corrosion products. These results confirm the superior passivating behavior of the zinc coating [44,45].

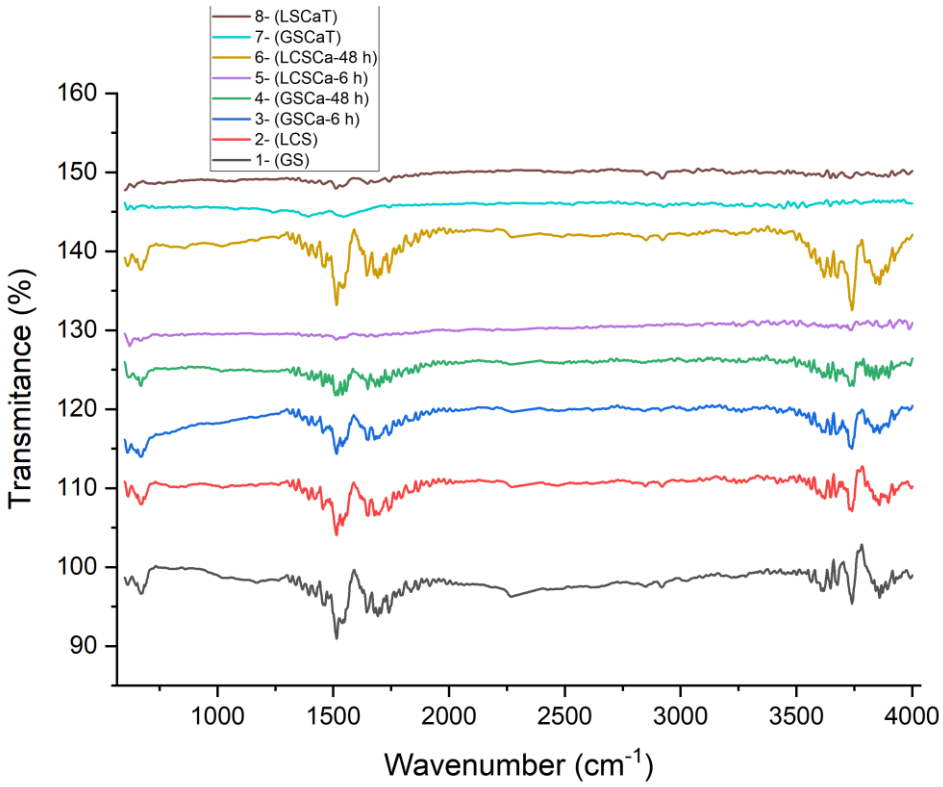

Figure 8 FTIR spectra of galvanized steel (GS), low-carbon steel (LCS), and their citric-acid-treated and polarized samples: (1) GS, (2) LCS, (3) GSCa-6 h, (4) GSCa-48 h, (5) LCSCa-6 h, (6) LCSCa-48 h, (7) GSCaT, and (8) LSCaT.

3.6. Effect of nanotechnology on corrosion resistance

Nanotechnology significantly enhances corrosion resistance by refining microstructure and improving passive film characteristics. Nanostructured coatings exhibit higher density, reduced porosity, and improved adhesion, which limit the penetration of corrosive species. Compared to conventional galvanized coatings, nano-enhanced surfaces provide superior electrochemical stability and long-term protection in acidic environments (Table 3) [13].

Table 3 Comparison between conventional and nanotechnology-enhanced corrosion protection systems for steel in acidic environments.

Parameter	Conventional Steel	Nano-Enhanced Steel
Corrosion Rate	Moderate	Reduced
Passive Film Stability	Moderate	High
Surface Uniformity	Moderate	High
Porosity	Higher	Reduced
Durability	Moderate	Enhanced

Figure 9 presents the improvement in corrosion resistance due to nanotechnology, highlighting reduced corrosion rate and enhanced passive film stability.

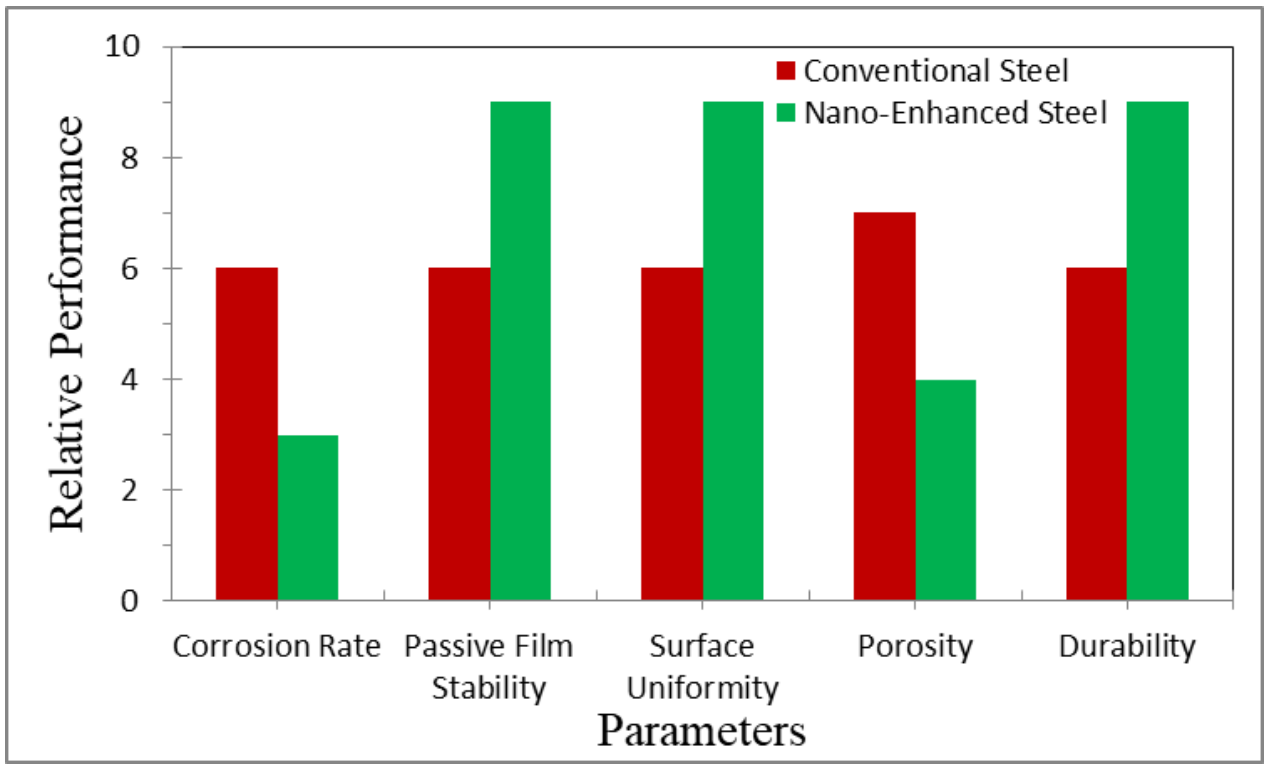

Figure 9 Graphical comparison of corrosion performance between conventional and nanotechnology-enhanced steel, illustrating improved resistance and reduced degradation.

4. CONCLUSIONS

This study demonstrates clear differences in the corrosion behavior of galvanized steel (GS) and low-carbon steel (LCS) in a citric acid solution (pH = 3), governed by their surface chemistry and oxide layer stability. Gravimetric and electrochemical results show strong agreement, confirming the reliability of the experimental approaches. GS exhibited an initially higher corrosion rate that

decreased significantly with time due to the formation of a stable and adherent ZnO/$Zn(OH)_2$ passive film, as supported by Tafel polarization, XRD, FTIR, and optical microscopy analyses. In contrast, LCS showed a gradual increase in corrosion rate resulting from the breakdown of its less protective iron oxide/hydroxide layers and the development of localized pitting. Microstructural refinement and increased microstrain observed in GS further contributed to its enhanced corrosion resistance. Overall, the zinc coating provides effective sacrificial protection and long-term durability in acidic environments, while bare low-carbon steel remains highly susceptible to acid-induced degradation, highlighting the importance of galvanization for corrosion mitigation. The integration of nanotechnology into corrosion protection strategies offers significant improvements in steel durability and performance. Nanostructured coatings enhance passive film stability, reduce corrosion rates, and improve long-term resistance in acidic environments. Future research should focus on optimizing nano-based coatings for industrial applications.

References

[1] C. Soriano, Corrosion Science, 106 (2016) 373. https://doi.org/10.1016/j.corsci.2016.02.020
[2] I. Ezzeldin, Buildings, 14 (2024) 1066. https://doi.org/10.3390/buildings14041066
[3] S. Suganya, R. Jeyalakshmi, Materials Today: Proceedings (2021). https://doi.org/10.1016/j.matpr.2021.05.152
[4] G. Pacchioni, ACS Catalysis, 14 (2024) 2730. https://doi.org/10.1021/acscatal.3c05669
[5] A. Chaouki, et al., ACS Omega, 10 (2025). https://doi.org/10.1021/acsomega.5
[6] A. I. A. Ali, M. RASHEED, Experimental and Theoretical NANOTECHNOLOGY, 10 (2026) 239. https://doi.org/10.56053/10.s.239
[7] A. I. A. Ali, M. RASHEED, Experimental and Theoretical NANOTECHNOLOGY, 10 (2026) 277. https://doi.org/10.56053/10.s.277
[8] A. Khaleefah, M. RASHEED, Experimental and Theoretical NANOTECHNOLOGY, 10 (2026) 289. https://doi.org/10.56053/10.s.289
[9] W. Yuan, et al., Coatings, 11 (2021) 202. https://doi.org/10.3390/coatings11020202
[10] F. Boudou, et al., Notulae Scientia Biologicae, 17 (2025) 12593. https://doi.org/10.55779/nsb17312593
[11] H. Liu, et al., Journal of Physics: Conference Series, 2390 (2022) 012007. https://doi.org/10.1088/1742-6596/2390/1/012007
[12] I. M. Mohammed, M. Rasheed, AIP Conference Proceedings, 3321 (2025) 020026. https://doi.org/10.1063/5.0289719
[13] P. Dhull, et al., Chemosphere, 333 (2023) 138873. https://doi.org/10.1016/j.chemosphere.2023.138873
[14] L. Hoang, et al., Sensors and Actuators B: Chemical, 348 (2021) 130684. https://doi.org/10.1016/j.snb.2021.130684
[15] Z. Yu, H. Gao, Frontiers in Materials, 7 (2020) 74. https://doi.org/10.3389/fmats.2020.00074.
[16] M. G. Jiru, M. A. Tolcha, D. A. Yeshanew, Journal of Basic & Applied Sciences, 17 (2021) 95. https://doi.org/10.29169/1927-5129.2021.17.11
[17] A. Zubaidi, L. M. Asaad, I. Alshalal, M. Rasheed, Journal of the Mechanical Behavior of Materials, 32 (2023) 1. https://doi.org/10.1515/jmbm-2022-0302
[18] A. Ashraf, R. Rashid, R. Nawaz, O. Alabdali, N. Fewster-Young, A. H. Ali, F. Ghanim, A. Alb Lupaş, Fractal and Fractional, 7 (2023) 673. https://doi.org/10.3390/fractalfract7090673
[19] J. A. Ghani, F. M. Yusop, A. Ismail, T. Noor, Materials Today: Proceedings (2024). https://doi.org/10.1016/j.matpr.2024.01.024

[20] R. S. Mahmood, et al., Journal of the Mechanical Behavior of Materials, 34 (2025) 1. https://doi.org/10.1515/jmbm-2025-0040
[21] M. Rasheed, A. Khaleefah, Materials Chemistry and Physics, 355 (2026) 132112. https://doi.org/10.1016/j.matchemphys.2026.132112
[22] M. Rasheed, et al., Journal of Advanced Biotechnology and Experimental Therapeutics, 6 (2023) 495. https://doi.org/10.5455/jabet.2023.d144
[23] E. Kadri, et al., Journal of Alloys and Compounds, 705 (2017) 708. https://doi.org/10.1016/j.jallcom.2017.02.117
[24] M. Rasheed, R. Barillé, Journal of Alloys and Compounds, 728 (2017) 1186. https://doi.org/10.1016/j.jallcom.2017.09.084
[25] H. K. Aity, M. Rasheed, E. Dhahri, A. A. Hateef, T. Saidani, Journal of Materials Science, 61 (2026) 6226. https://doi.org/10.1007/s10853-026-12241-w
[26] S. S. Batros, M. Rasheed, H. K. Aity, A. A. Hatef, T. Saidani, Materials Chemistry and Physics, 355 (2026) 132243. https://doi.org/10.1016/j.matchemphys.2026.132243
[27] T. Saidani, M. Rasheed, I. Alshalal, A. A. Rashed, M. A. Sarhan, R. Barillé, Research on Engineering Structures and Materials, 9 (2023) 1. https://doi.org/10.17515/resm2023.21ma0922rs
[28] M. Rasheed, O. Y. Mohammed, S. Shihab, A. Al-Adili, Journal of Physics: Conference Series, 1795 (2021) 012042. https://doi.org/10.1088/1742-6596/1795/1/012042
[29] A. Raghdi, M. Heraiz, M. Rasheed, A. Keziz, Journal of the Indian Chemical Society, 101 (2024) 101413. https://doi.org/10.1016/j.jics.2024.101413
[30] F. Boudou, A. E. Sabar, M. I. Majeed, A. M. Ibraham, R. Jamal, A. Rashid, A. Belakredar, M. Bendahmane-Salmi, M. RASHEED, R. RASHEED, T. Saidani, H. D. Al-Bahadli, Experimental and Theoretical NANOTECHNOLOGY, 10 (2026) 821. https://doi.org/10.56053/10.S.821
[31] D. Kherifi, A. Keziz, M. Rasheed, A. Oueslati, Ceramics International, 50 (2024) 1. https://doi.org/10.1016/j.ceramint.2024.05.317
[32] M. Rasheed, S. Shihab, O. Alabdali, A. Rashid, T. Rashid, Journal of Physics: Conference Series, 1999 (2021) 012077. https://doi.org/10.1088/1742-6596/1999/1/012077
[33] K. K. Khudair, F. Boudou, A. Mohammed, A. Sehmi, A. Belakredar, M. S. Ibrahim, Experimental and Theoretical NANOTECHNOLOGY, 10 (2026) 869. https://doi.org/10.56053/10.S.869
[34] E. Kadri, M. Krichen, R. Mohammed, A. Zouari, K. Khirouni, Optical and Quantum Electronics, 48 (2016) 1. https://doi.org/10.1007/s11082-016-0812-7
[35] H. K. Aity, E. Dhahri, M. Rasheed, Ceramics International, 50 (2024) 54666. https://doi.org/10.1016/j.ceramint.2024.10.324
[36] M. S. Ibrahim, T. T. Issa, B. Yaqoob, E. N. Fayyadh, A. Rashid, R. S. Mahmood, Experimental and Theoretical NANOTECHNOLOGY, 10 (2026) 887. https://doi.org/10.56053/10.S.887
[37] Z. S. Ahmed, M. RASHEED, H. S. Ahmed, Experimental and Theoretical NANOTECHNOLOGY, 10 (2026) 329. https://doi.org/10.56053/10.s.329
[38] Z. S. Ahmed, M. RASHEED, H. S. Ahmed, Experimental and Theoretical NANOTECHNOLOGY, 10 (2026) 343. https://doi.org/10.56053/10.s.343
[39] E. Arif, R. Jamal, M. RASHEED, Experimental and Theoretical NANOTECHNOLOGY, 10 (2026) 453. https://doi.org/10.56053/10.2.453
[40] G. E. Alkinani, A. R. J. Katae, M. RASHEED, Experimental and Theoretical NANOTECHNOLOGY, 10 (2026) 1027. https://doi.org/10.56053/10.S.1027
[41] A. Keziz, M. Rasheed, M. Heraiz, F. Sahnoune, A. Latif, Ceramics International, 49 (2023) 37423. https://doi.org/10.1016/j.ceramint.2023.09.068
[42] A. A. Hateef, E. Dhahri, M. Rasheed, H. Kadhim, Z. Abbas, N. Hassan, Physics and Chemistry of Solid State, 25 (2024) 801. https://doi.org/10.15330/pcss.25.4.801-810

[43] T. Saidani, S. Mokhtari, M. Rasheed, H. Lahmar, M. Trari, Journal of the Indian Chemical Society, 103 (2026) 102499. https://doi.org/10.1016/j.jics.2026.102499
[44] A. J. Hussein, M. N. Al-Darraji, M. Rasheed, IOP Conference Series: Earth and Environmental Science, 1262 (2023) 022007. https://doi.org/10.1088/1755-1315/1262/2/022007
[45] T. Rashid, M. M. Mokji, M. Rasheed, Journal of Optics, 53 (2024) 1. https://doi.org/10.1007/s12596-024-02080-w
[46] A. A. Abdulrahman, M. Rasheed, S. Shihab, Journal of Physics: Conference Series, 1879 (2021) 022118. https://doi.org/10.1088/1742-6596/1879/2/022118
[47] T. Rashid, M. M. Mokji, M. Rasheed, Journal of the Mechanical Behavior of Materials, 34 (2025) 1. https://doi.org/10.1515/jmbm-2025-0074
[48] M. Enneffati, M. Rasheed, B. Louati, K. Guidara, R. Barillé, Optical and Quantum Electronics, 51 (2019) 1. https://doi.org/10.1007/s11082-019-2015-5
[49] A. Jaber, M. Ismael, T. Rashid, M. A. Sarhan, M. Rasheed, I. M. Sala, Eureka: Physics and Engineering, 4 (2023) 29. https://doi.org/10.21303/2461-4262.2023.002770
[50] A. J. Hussein, M. N. Al-Darraji, M. Rasheed, M. A. Sarhan, IOP Conference Series: Earth and Environmental Science, 1262 (2023) 022005. https://doi.org/10.1088/1755-1315/1262/2/022005
[51] M. Rasheed, I. Alshalal, A. A. Rashed, M. A. Sarhan, A. S. Jaber, Indonesian Journal of Electrical Engineering and Computer Science, 33 (2024) 653. https://doi.org/10.11591/ijeecs.v33.i1.pp653-660
[52] M. Rasheed, M. N. Mohammedali, F. A. Sadiq, M. A. Sarhan, T. Saidani, Journal of Optics, 54 (2024) 1. https://doi.org/10.1007/s12596-024-01928-5
[53] A. R. J. Katae, H. H. Hussein, A. S. Jaber, M. A. Sarhan, M. RASHEED, Experimental and Theoretical NANOTECHNOLOGY, 10 (2026) 795. https://doi.org/10.56053/10.2.795
[54] A. R. J. Katae, H. H. Hussein, A. S. Jaber, M. A. Sarhan, M. RASHEED, Experimental and Theoretical NANOTECHNOLOGY, 10 (2026) 725. https://doi.org/10.56053/10.2.725
[55] H. M. I. Al-Zuhairi, I. Alshalal, H. H. Abbood, M. Al Nuaimi, Experimental and Theoretical NANOTECHNOLOGY, 10 (2026) 855. https://doi.org/10.56053/10.S.855
[56] H. M. I. Al-Zuhairi, I. Alshalal, H. H. Abbood, M. Al Nuaimi, Experimental and Theoretical NANOTECHNOLOGY, 10 (2026) 1093. https://doi.org/10.56053/10.S.1093
[57] W. Saidi, N. Hfaidh, M. Rasheed, M. Girtan, A. Megriche, M. El Maaoui, RSC Advances, 6 (2016) 68819. https://doi.org/10.1039/c6ra15060h
[58] M. Enneffati, B. Louati, K. Guidara, M. Rasheed, R. Barillé, Journal of Materials Science: Materials in Electronics, 29 (2018) 171. https://doi.org/10.1007/s10854-017-7901-7
[59] F. Dkhilalli, S. Megdiche, K. Guidara, M. Rasheed, R. Barillé, M. Megdiche, Ionics, 24 (2018) 169. https://doi.org/10.1007/s11581-017-2193-8
[60] F. Boudou, A. Guendouzi, A. Belakredar, M. RASHEED, Notulae Scientia Biologicae, 16 (2024) 13837. https://doi.org/10.55779/nsb16211837
[61] F. Boudou, A. Belakredar, A. Berkane, M. RASHEED, Notulae Scientia Biologicae, 17 (2025) 12183. https://doi.org/10.55779/nsb17212183
[62] A. Aukštuolis, et al., Proceedings of the Romanian Academy Series A: Mathematics, Physics, Technical Sciences, Information Science, 18 (2017) 34. https://hal.archives-ouvertes.fr/hal-02443179
[63] T. Saidani, M. Zaabat, M. S. Aida, R. Barillé, M. Rasheed, Y. Almohamed, Journal of Materials Science: Materials in Electronics, 28 (2017) 9252. https://doi.org/10.1007/s10854-017-6660-9